

Universal Prony fitting decomposition for optimized hierarchical quantum master equations

Zi-Hao Chen, Yao Wang, Xiao Zheng, Rui-Xue Xu, and YiJing Yan*

Department of Chemical Physics, University of Science and Technology of China, Hefei, Anhui 230026, China

(Dated: April 15, 2022)

In this work, we propose the Prony fitting decomposition (PFD) as an accurate and efficient exponential series method, applicable to arbitrary interacting bath correlation functions. The resulting hierarchical equations of motion (HEOM) formalism is greatly optimized, especially in extremely low temperature regimes that would be inaccessible with other methods. For demonstration, we calibrate the present PFD against the celebrated Padé spectrum decomposition method, followed by converged HEOM evaluations on the single-impurity Anderson model system.

Dissipation is ubiquitous in almost all realms of modern physics. Various quantum dissipation theories (QDTs) are exploited to deal with the reduced system dynamics. Almost all QDTs are based on the Gaussian environment description, whose influence can be completely dictated by the interacting bath correlation function, $C_B(t)$. Theoretical methods, such as hierarchical equations of motion (HEOM), [1–8] quantum Monte Carlo [9] and numerical renormalization group, [10] are heavily based on the efficiency of exponential series expansion,

$$C_B(t) = \frac{1}{\pi} \int_{-\infty}^{\infty} d\omega e^{\pm i\omega t} J(\omega) f^{F/B}(\omega) \simeq \sum_{k=1}^K \eta_k e^{-\gamma_k t}. \quad (1)$$

The first identity is the fluctuation–dissipation theorem, involving $J(\omega)$, the interacting bath spectrum density, and $f^{F/B}(\omega)$, the Fermi/Bose function. The second identity arises from certain sum–over–poles (SOP) scheme, followed by Cauchy’s contour integration. In convention, $f^{F/B}(\omega)$ is the quantity of the SOP decomposition, since $J(\omega)$ is often given with models. By far the Padé spectrum decomposition (PSD) is the golden standard scheme, [11, 12] except for the extremely low–temperature regime, due to the underlying discontinuity that leads to the accuracy length of effective $f^{F/B}(\omega)$ shrinking intensely. Alternative methods include the Fano spectrum decomposition, [13, 14] discrete Fourier series [15] and extended orthogonal polynomials expansions. [16–20]

In this work, we propose the Prony fitting decomposition (PFD) scheme, directly for the second identity of Eq. (1). As known, optimized Prony fitting method [21] has been exploited in other fields of physics. Note that $C_B(t) \equiv C_B^{(r)}(t) + iC_B^{(i)}(t)$, with the temperature dependence appearing only in one of the parts. It is the imaginary part for the fermionic case, while the bosonic case is the opposite. Naturally, the numerical fit is to be performed against the exact $C_B(t)$ satisfying the first identity of Eq. (1), the fluctuation–dissipation theorem.

We will see that PFD is superb, covering extremely low–temperature regimes and also rather arbitrary spectral densities. The resulting PFD–HEOM shows a greatly enhanced range of applications. The proposed PFD, exemplified with the fermionic case detailed in the caption of Fig. 1, targets at optimizing K_i in

$$C_B^{(i)}(t) \equiv \text{Im} C_B(t) = \sum_{k=1}^{K_i} \zeta_k e^{-\lambda_k t}. \quad (2)$$

The total $K = K_r + K_i$, where K_r is via the real part fitting. Its protocol goes as follows.

(1) Sample the exact and temperature dependent $C_B^{(i)}(t)$ to obtain

$$\phi_j \equiv C_B^{(i)}(jdt); \quad j = 0, \dots, 2N. \quad (3)$$

Here, $dt \equiv t_c/(2N)$ with t_c being the cutoff time of $C_B^{(i)}(t)$. For demonstrations, we set $N = 15000$ and $t_c = 80\Delta^{-1}$, where Δ stands for the characteristic width of $J(\omega)$; see the caption of Fig. 1 for the details.

(2) Construct the $(N + 1) \times (N + 1)$ Hankel matrix,

$$\mathbf{H} = \begin{bmatrix} \phi_0 & \phi_1 & \cdots & \phi_N \\ \phi_1 & \phi_2 & \cdots & \phi_{N+1} \\ \dots & \dots & \dots & \dots \\ \phi_N & \phi_{N+1} & \cdots & \phi_{2N} \end{bmatrix}. \quad (4)$$

(3) Decompose \mathbf{H} with the Takagi’s factorization,

$$\mathbf{H}\mathbf{u}_m = \sigma_m \mathbf{u}_m^*; \quad m = 0, \dots, N. \quad (5)$$

Here, \mathbf{u}_m^* is complex conjugate of $\mathbf{u}_m \equiv \{u_{0m}, \dots, u_{Nm}\}$. The obtained σ_m and \mathbf{u}_m are called c-eigenvalues and c-eigenvectors in literature. We order $\{\sigma_m\}$ according to the descending $|\sigma_m|$ -values and $\{\mathbf{u}_m\}$ just follows. In most cases, $\{|\sigma_m|\}$ descend rapidly; see Fig. 1(a).

(4) Upon the above setup, we select $\mathbf{u}_{m=K_i}$ to define

$$f(z) \equiv \sum_{n=0}^N u_{nK_i} z^n. \quad (6)$$

Then obtain the $N + 1$ roots, w_0, \dots, w_N , of this polynomial. As known [21], K_i roots are of $|w_k| < 1$, whereas

*Electronic address: yanyj@ustc.edu.cn

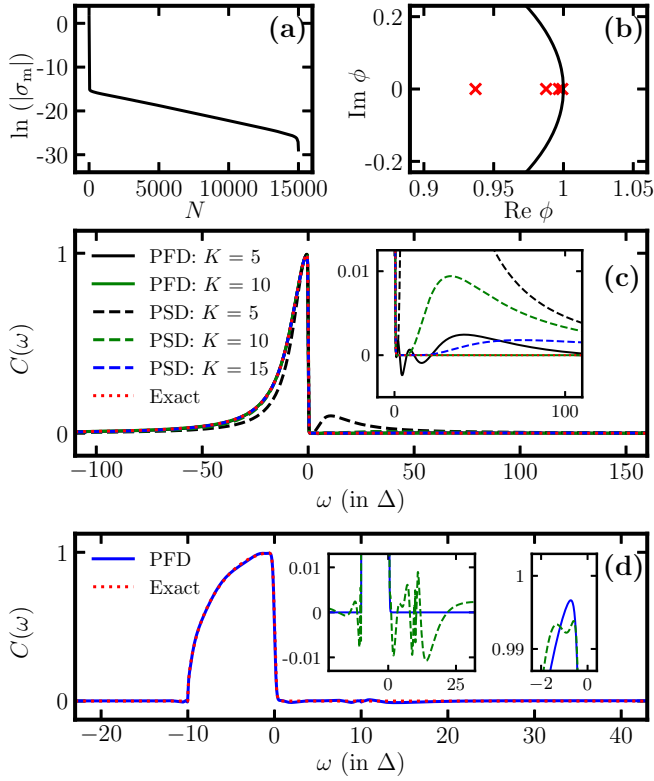


FIG. 1: An illustrative example of PFD scheme. In panels (a), (b) and (c), the Lorentzian spectral density is adopted with $W = 10\Delta$ and $\beta\Delta = 10$ [cf. Eq. (9)]. In (d), the semicircle $J(\omega)$ is adopted [cf. Eq. (11)]. In panels (a) and (b), the illustrations of step (3) and (4) of the PFD scheme, respectively, with $K_r = 1$ and $K_i = 4$. In panels (c) and (d), the fitting results are shown explicitly with the spectrum $C(\omega)$ [cf. Eq. (10)].

others are setting in the unit circle; see red cross marks in Fig. 1(b). Now we obtain the exponents $\{\lambda_1, \dots, \lambda_{K_i}\}$ in Eq. (2) as

$$\lambda_k = -\frac{2N}{t_c} [\ln |w_k| + i \arg(w_k)], \quad (7)$$

where $\arg(w_k) \in (-\pi, \pi]$.

(5) Obtain $\{\zeta_1, \dots, \zeta_K\}$ in Eq. (2) by the least-squares fitting the following $2N + 1$ equations,

$$\phi_j = \sum_{k=1}^{K_i} \zeta_k w_k^j; \quad j = 0, \dots, 2N. \quad (8)$$

Involved are those K_i roots of $|w_k| < 1$; see the remarks after Eq. (7).

(6) Treat $C_B^{(r)}(t)$, following the same procedure above. Resulting in total $K = K_r + K_i$ terms in Eq. (1). This finalizes the PFD steps.

Some worthy remarks are as follows: (i) The exponents, $\{\lambda_k\}$ in Eq. (2) with Eq. (7), are either real or in complex conjugate pairs. This property is required by the

underlying time-reversal symmetry in Eq. (1); (ii) Generally speaking, both $C_B^{(r)}(t)$ and $C_B^{(i)}(t)$ require PFD, except for some special cases. Demonstrated in Fig. 1(c) and (d) are the Lorentzian and semicircle spectral densities. In the former case, the $C_B^{(r)}(t)$ can be obtained as a single exponential term analytically, and needs no fitting treatment. This simply leads to $K_r = 1$. While in the later case, both $C_B^{(r)}(t)$ and $C_B^{(i)}(t)$ need fitting; (iii) The PFD results for Lorentzian spectral density,

$$J(\omega) = \frac{\Delta W^2}{\omega^2 + W^2}, \quad (9)$$

compared with the PSD schemes, are illustrated in Fig. 1; see black the solid and dash lines in panel (c). Exhibited in Fig. 1(c) are also other different choices of K . They are explicitly shown with the spectrum,

$$C(\omega) = \frac{1}{2} \int_{-\infty}^{\infty} dt e^{-i\omega t} C_B^{(r)}(t). \quad (10)$$

It can be found that errors primarily occur near the zero frequency. We will compare the performances of PFD and PSD quantitatively below in Fig. 2.

As an example of non-analytical spectral density cases, we also apply the PFD scheme to semicircle spectral density [cf. the inserted subfigure of Fig. 3(b)],

$$J(\omega) = \begin{cases} \Delta \sqrt{1 - (\omega/W)^2}, & -W \leq \omega \leq W, \\ 0, & \omega < -W \text{ or } \omega > W. \end{cases} \quad (11)$$

The fitting result are shown in Fig. 1(d). Notice that the PSD method is absent due to its failure in this case of spectral density. We fit the real part with $K_r = 7$ and the imaginary part with $K_i = 8$, respectively.

In Fig. 2, we calibrate the relationships between the accuracy and K for Lorentzian spectral density at different temperatures. The fitting errors are measured by

$$\text{Error} = \frac{\int_{-\infty}^{\infty} d\omega |C_B^{\text{fit}}(\omega) - C_B(\omega)|}{\int_{-\infty}^{\infty} d\omega |C_B(\omega)|}. \quad (12)$$

We observe that at the same accuracy level, PFD requires 1/16, 1/8 and 1/4 summation terms of that required by PSD when $\beta\Delta = 1000, 100$ and 10, respectively. This is exactly what we need for overcoming the low-temperature curse encountered in HEOM simulations. The PFD scheme remarkably reduces the computational and memory costs. In the fermionic HEOM evaluations, the number of involved auxiliary density operators is

$$\mathcal{N} = \sum_{l=1}^L \frac{\tilde{K}!}{l!(\tilde{K}-l)!} \quad (13)$$

where L is the tier of hierarchy truncation and the total number of involved exponential terms is $\tilde{K} = 2 \times N_\alpha \times N_u \times K$, with N_α and N_u being the numbers of bath reservoirs and system orbitals, respectively. The factor of 2

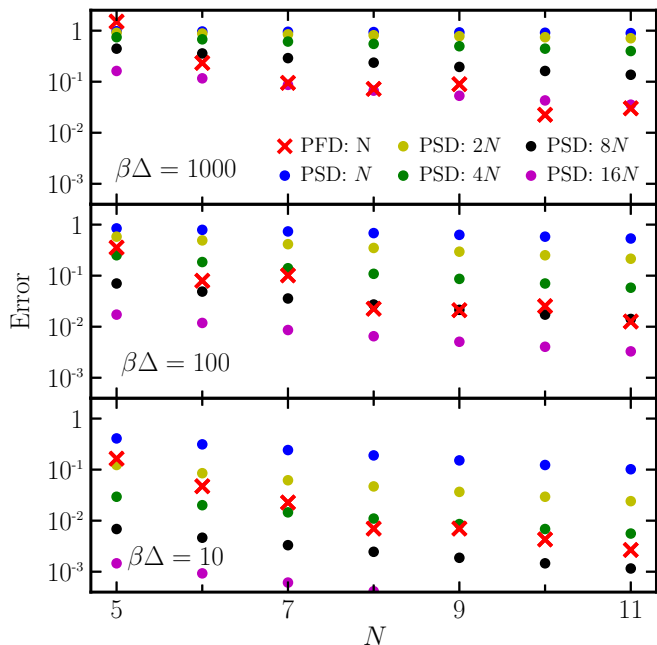


FIG. 2: Performances of the PFD compared with PSD at different temperatures: $\beta\Delta = 1000$, 100 and 10. We adopt the Lorentzian form of spectral density with $W = 10\Delta$.

accounts for particles plus holes. To be concrete, when the L is 6, PFD requires only 10^{-7} , 10^{-5} , 10^{-4} computational and memory costs of that required by PSD when $\beta\Delta = 1000$, 100 and 10 [cf. Eq. (13)].

As a numerical demonstration, we exploit the PFD scheme in the HEOM simulations of SIAM. [22–26] SIAM is frequently exploited to study the the Kondo resonance, which is massively investigated since it manifests strong electronic correlations at very low temperatures. Its Hamiltonian reads

$$H_T = H_S + H_{SB} + h_B, \quad (14)$$

where the system is

$$H_S = \epsilon(\hat{n}_\uparrow + \hat{n}_\downarrow) + U\hat{n}_\uparrow\hat{n}_\downarrow \quad (15)$$

with $\hat{n}_s = \hat{a}_s^\dagger\hat{a}_s$, the system–environment interaction reads

$$H_{SB} = \sum_k \sum_{s=\uparrow,\downarrow} t_{ks}(\hat{a}_s^\dagger\hat{d}_{ks} + \text{H.c.}), \quad (16)$$

and the environment, $h_B = \sum_{ks} \epsilon_{ks}\hat{d}_{ks}^\dagger\hat{d}_{ks}$, is composed of free elections. In simulation, we select SIAM parameters to be $U = 12\Delta$ and $\epsilon = -U/2$, and the Kondo temperate is around $\beta\Delta = 40$.

The simulation results are exhibited with impurity spectral density

$$A_s(\omega) = \frac{1}{2\pi} \int_{-\infty}^{\infty} dt e^{i\omega t} \langle \{\hat{a}_s(t), \hat{a}_s^\dagger(0)\} \rangle, \quad (17)$$

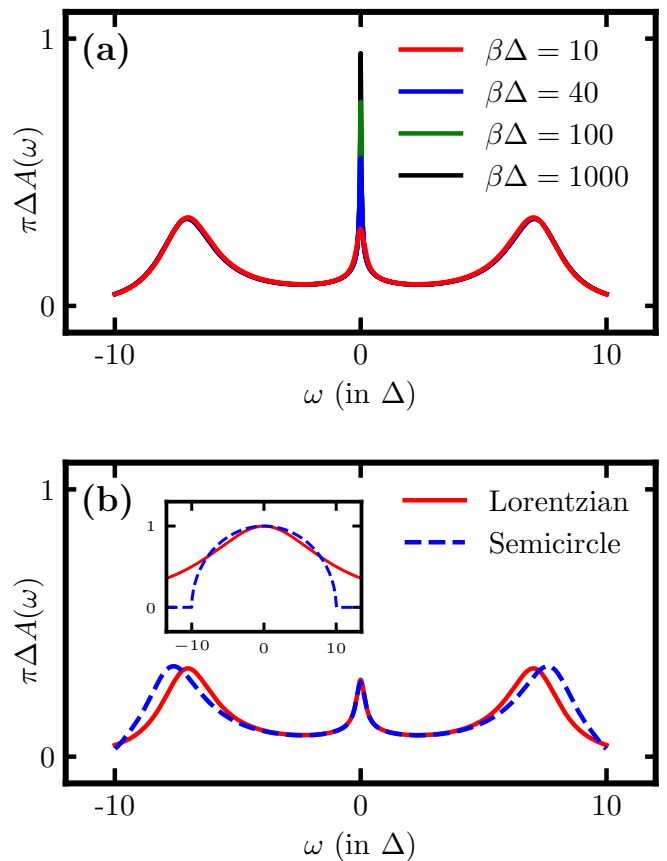


FIG. 3: The HEOM simulation results of $\Delta A(\omega)$ with different types of spectral densities. In panel (a), we apply the Lorentzian spectral density with $W = 10\Delta$. Temperatures are $\beta\Delta = 10, 40, 100$ and 1000. Other parameters are: $U = 12\Delta$ and $\epsilon = -U/2$. In panel (b) we compare the result of $A(\omega)$ with the Lorentzian versus semicircle spectral densities (cf. the inserted subfigure) in the case of $\beta\Delta = 10$.

where \hat{a}_s (\hat{a}_s^\dagger) is the creation (annihilation) operator of the electron with spin s . The HEOM simulation results of $\Delta A(\omega)$ with Lorentzian spectral densities are shown in Fig. 3(a) at different temperatures: $\beta\Delta = 10, 40, 100$ and 1000 are shown in Fig. 3. In these simulations, the number of exponential terms, K in Eq. (1), is 5, 6, 8 and 10 respectively, and we set the truncation tier to be $L = 6$. As expected, the Kondo peak $\pi\Delta A(0)$ increase to 1 as the temperature decrease to 0. This behavior agrees with the Friedel sum rule [27] at zero temperature, $A(0) = \sin^2(\pi\bar{n})/(\pi\Delta)$, where \bar{n} is the average electron occupation number. It is also observed that the Hubbard peaks occurs at $\omega = \pm U/2$, and the these peak are almost not affected by temperature. In Fig. 3(b), we compare the simulation results of $A(\omega)$ with the Lorentzian versus semicircle spectral densities. As shown in the figure, the difference appears apparently near the Hubbard peaks.

In summary, we propose the PFD scheme to accurately decompose the environment correlation functions into exponential sums. This scheme significantly improves the

efficiency and applicability of HEOM. It not only helps reduce the numerical costs at extremely low temperatures, but also enables HEOM to deal with analytical spectral densities. We exhibit and calibrate the PFD scheme in fermionic scenario and take the SIAM as an example. It is anticipated that the PSD scheme will greatly benefit the HEOM simulation at cryogenic temperatures.

Support from the Ministry of Science and Tech-

nology of China (Grant No. 2017YFA0204904 and 2021YFA1200103) and the National Natural Science Foundation of China (Grant Nos. 22103073 and 22173088) is gratefully acknowledged. Y. Wang and Z. H. Chen thank also the partial support from GHfund B (20210702). We are indebted to Yu Su for valuable discussions.

-
- [1] Y. Tanimura, “Nonperturbative expansion method for a quantum system coupled to a harmonic-oscillator bath,” *Phys. Rev. A* **41**, 6676 (1990).
- [2] Y. Tanimura, “Stochastic Liouville, Langevin, Fokker-Planck, and master equation approaches to quantum dissipative systems,” *J. Phys. Soc. Jpn.* **75**, 082001 (2006).
- [3] Y. A. Yan, F. Yang, Y. Liu, and J. S. Shao, “Hierarchical approach based on stochastic decoupling to dissipative systems,” *Chem. Phys. Lett.* **395**, 216 (2004).
- [4] R. X. Xu, P. Cui, X. Q. Li, Y. Mo, and Y. J. Yan, “Exact quantum master equation via the calculus on path integrals,” *J. Chem. Phys.* **122**, 041103 (2005).
- [5] R. X. Xu and Y. J. Yan, “Dynamics of quantum dissipation systems interacting with bosonic canonical bath: Hierarchical equations of motion approach,” *Phys. Rev. E* **75**, 031107 (2007).
- [6] J. S. Jin, X. Zheng, and Y. J. Yan, “Exact dynamics of dissipative electronic systems and quantum transport: Hierarchical equations of motion approach,” *J. Chem. Phys.* **128**, 234703 (2008).
- [7] L. Z. Ye, X. L. Wang, D. Hou, R. X. Xu, X. Zheng, and Y. J. Yan, “HEOM-QUICK: A program for accurate, efficient and universal characterization of strongly correlated quantum impurity systems,” *WIREs Comp. Mol. Sci.* **6**, 608 (2016).
- [8] Y. A. Yan and J. S. Shao, “Stochastic description of quantum Brownian dynamics,” *Front. Phys.* **11**, 110309 (2016).
- [9] E. Gull, A. J. Millis, A. I. Lichtenstein, A. N. Rubtsov, M. Troyer, and P. Werner, “Continuous-time Monte Carlo methods for quantum impurity models,” *Rev. Mod. Phys.* **83**, 349 (2011).
- [10] Ž. Osolin et al., “Padé approximant approach for obtaining finite-temperature spectral functions of quantum impurity models using the numerical renormalization group technique,” *Phys. Rev. B* **87**, 245135 (2013).
- [11] J. Hu, R. X. Xu, and Y. J. Yan, “Padé spectrum decomposition of Fermi function and Bose function,” *J. Chem. Phys.* **133**, 101106 (2010).
- [12] J. Hu, M. Luo, F. Jiang, R. X. Xu, and Y. J. Yan, “Padé spectrum decompositions of quantum distribution functions and optimal hierarchical equations of motion construction for quantum open systems,” *J. Chem. Phys.* **134**, 244106 (2011).
- [13] L. Cui, H. D. Zhang, X. Zheng, R. X. Xu, and Y. J. Yan, “Highly efficient and accurate sum-over-poles expansion of Fermi and Bose functions at near zero temperatures: Fano spectrum decomposition scheme,” *J. Chem. Phys.* **151**, 024110 (2019).
- [14] H. D. Zhang, L. Cui, H. Gong, R. X. Xu, X. Zheng, and Y. J. Yan, “Hierarchical equations of motion method based on Fano spectrum decomposition for low temperature environments,” *J. Chem. Phys.* **152**, 064107 (2020).
- [15] Y. Zhou and J. S. Shao, “Solving the spin-boson model of strong dissipation with flexible random-deterministic scheme,” *J. Chem. Phys.* **128**, 034106 (2008).
- [16] H. Liu, L. L. Zhu, S. M. Bai, and Q. Shi, “Reduced quantum dynamics with arbitrary bath spectral densities: Hierarchical equations of motion based on several different bath decomposition schemes,” *J. Chem. Phys.* **140**, 134106 (2014).
- [17] Z. F. Tang, X. L. Ouyang, Z. H. Gong, H. B. Wang, and J. L. Wu, “Extended hierarchy equation of motion for the spin-boson model,” *J. Chem. Phys.* **143**, 224112 (2015).
- [18] K. Nakamura and Y. Tanimura, “Hierarchical Schrödinger equations of motion for open quantum dynamics,” *Phys. Rev. A* **98**, 012109 (2018).
- [19] T. Ikeda and G. D. Scholes, “Generalization of the hierarchical equations of motion theory for efficient calculations with arbitrary correlation functions,” *J. Chem. Phys.* **152**, 204101 (2020).
- [20] N. Lambert, S. Ahmed, M. Cirio, and F. Nori, “Modelling the ultra-strongly coupled spin-boson model with unphysical modes,” *Nature Comm.* **10**, 3721 (2019).
- [21] G. Beylkin and L. Monzón, “On approximation of functions by exponential sums,” *Appl. Comput. Harmon. Anal.* **19-1**, 17 (2005).
- [22] W. Liang, M. P. Shores, M. Bockrath, J. R. Long, and H. Park, “Kondo resonance in a single-molecule transistor,” *Nature* **417**, 725 (2002).
- [23] L. Farinacci, G. Ahmadi, M. Ruby, G. Reecht, B. W. Heinrich, C. Czekelius, F. von Oppen, and K. J. Franke, “Interfering tunneling paths through magnetic molecules on superconductors: Asymmetries of Kondo and Yu-Shiba-Rusinov resonances,” *Phys. Rev. Lett.* **125**, 256805 (2020).
- [24] C. P. Moca, I. Weymann, M. A. Werner, and G. Zaránd, “Kondo cloud in a superconductor,” *Phys. Rev. Lett.* **127**, 186804 (2021).
- [25] A. Kurzman, Y. Kleorin, C. Tong, R. Garreis, A. Knothe, M. Eich, C. Mittag, C. Gold, F. K. de Vries, K. Watanabe, T. Taniguchi, V. Falko, Y. Meir, T. Ihn, and K. Ensslin, “Kondo effect and spin-orbit coupling in graphene quantum dots,” *Nat. Comm.* **12**, 1 (2021).
- [26] M. Ferrier, R. Delagrè, J. Basset, H. Bouchiat, T. Arakawa, T. Hata, R. Fujiwara, Y. Teratani, R. Sakano, A. Oguri, K. Kobayashi, and R. Deblock, “Quantum noise in carbon nanotubes as a probe of correlations in the Kondo regime,” *J. Low Temp. Phys.* **201**, 738 (2020).
- [27] D. C. Langreth, “Friedel sum rule for Anderson’s model of localized impurity states,” *Phys. Rev.* **150**, 516 (1966).